Sensitivity Analysis of Relative Permeability on Unsteady-State Core Flooding via Experimental Data

Miquéias Mateus Ferreira Leite[1,2], Gianfranco de Mello Stieven[2,3], Filipe Oliveira da Silva[2,3], Caroline Henrique Dias[2], Rodrigo Surmas[4], Paulo Couto[1,2]

[1]*Programa de Engenharia Civil, Universidade Federal do Rio de Janeiro*
Av. Athos da Silveira Ramos, 149, 21941-909, Rio de Janeiro - RJ, Brasil
miqueiasmleite@coc.ufrj.br, pcouto@petroleo.ufrj.br
[2]*Laboratório de Recuperação Avançado de Petróleo (LRAP$^+$)*
R. Moniz de Aragão, 360, 21941-594, Rio de Janeiro - RJ, Brasil
miqueiasmleite@coc.ufrj.br, pcouto@petroleo.ufrj.br, filipe@petroleo.ufrj.br, stieven@petroleo.ufrj.br, caroldias@petroleo.ufrj.br
[3]*Programa de Engenharia Mecânica, Universidade Federal do Rio de Janeiro*
Av. Athos da Silveira Ramos, 149, 21941-909, Rio de Janeiro - RJ, Brasil
[4]*Centro de Pesquisas, Desnvolvimento e Inovação Leopoldo Américo Miguez de Mello - CENPES/PETROBRAS*
Av. Horácio Macedo, 950, Cidade Universitária 21941-915, Rio de Janeiro - RJ, Brasil surmas@petrobras.com.br

Abstract. Computational reservoir simulation is crucial for understanding fluid flow in geological formations, relying on parametric relations such as relative permeability (Krel) for modeling multiphase flow in porous media. These models often involve empirical parameters, necessitating parameter estimation and uncertainty quantification. However, sensitivity and linear dependence analysis are often neglected, especially in core flooding experiments. This study focuses on analyzing the reduced sensitivity coefficient of relative permeability parameters, using the LET model, in unsteady-state core-flooding experiments under different conditions. The experiments involve axial water injection into an oil-saturated plug, measuring the differencial pressure between the plug inlet and outlet and accumulated volume of oil produced. Based on experimental data, computational simulations were conducted using the Cydar® software to optimize the relative permeability and capillary pressure. The dynamic behavior of the relative permeability parameters' local sensitivity is showcased, alongside their dimensional comparison.

Keywords: Sensitivity Analysis; Relative Permeability; Advanced Oil Recovery; SCAL; Experimental Data.

1 Introduction

The development of advanced computational models enables the simulation of complex processes, providing precise analysis in porous media. The application of computational simulation in reservoir engineering is crucial for understanding reservoir geology and fluid flow analysis, enabling the development of advanced models and accurate predictions of fluid behavior in porous media [1].

These simulations use parametric models to represent the complex dynamics of characteristics, emphasizing the importance of relative permeability (Krel), a key rock-fluid parameter required for continuous-scale modeling of multiphase flow dynamics in porous media. Although different empirical formulations exist to characterize the water-oil relationship, the construction of these models generally relies on observations, theoretical reasoning, and heuristic concepts [2] .

Therefore, it becomes necessary to quantify the uncertainty associated with relative permeability. However, to achieve a satisfactory quantification of uncertainty, it is essential to investigate some aspects of these parameters, particularly regarding linear dependence and sensitivity.

Local sensitivity analysis can be useful for a variety of applications. For example, improve understanding of the relationships between input and output variables [3], determine which parts of the output variance are due to different inputs through index estimation [4], obtain essential information about the model's behavior, structure, and response to changes in input variables [5], test the robustness of model results in the presence of uncertainty [6], determine the influence of each parameter on the state variable and, consequently, its relevance in the optimization

process [7] and to enhance decision-making processes [8].

Methods like local sensitivity analysis provide means to explore the variability of model outputs in response to input factors, contributing to more reliable and precise results in petroleum reservoir modeling. In the aforementioned context of Krel, the model proposed by Lomeland et al. [9] is quite relevant due to its usual application on multiphase flow simulation in porous media. The LET model was developed to address the need to describe relative permeability curves across the entire saturation range, encompassing both low and high water saturations.

In this context, this study aims to analyze the reduced sensitivity coefficient of Krel, parameterized using the LET model, in unsteady-state core flooding experiments, taking into account multistep and single-step operating conditions, as well as capillary pressure parameterized by Log(beta) function [10].

2 Methodology

In this section, one describe the methodology applied in this study, focusing on the local sensitivity analysis method regarding the relative permeability parameters (Krel), considering experimental data including the pressure differential between water inlet and oil and water outlet (ΔP), along with the cumulative production (NP), and parameterized using the LET model. Additionally, the methodology takes into account the influence of capillary pressure, also parameterized by Log(beta) function [10].

2.1 Solution model

Inverse modeling is a fundamental technique for parameter inference in complex systems. In the context of two-phase flow, it allows the determination of reservoir properties, such as permeability and capillary pressure, from production and pressure data [11] [12].

Two-phase flow equations are derived from the mass conservation laws for each phase and are complemented by the generalized Darcy's law for two-phase flow. The interaction between phases is governed by capillary pressure and the relative permeability of each phase. For two-phase flow in porous media, these equations formulate the volumetric flux v_α(normalized by cross-sectional area) of phase where ($\alpha = \{w, n\}$) for wetting w and non-wetting phase n [12, 13], expressed as:

$$u_w = -\frac{kk_{rw}(S)}{\mu_w}\frac{\partial p_w}{\partial x}, \quad u_o = -\frac{kk_{ro}(S)}{\mu_o}\frac{\partial p_o}{\partial x} \tag{1}$$

where u_w and u_o represent the velocities of the wetting and non-wetting phases, respectively. The absolute permeability of the porous medium k determines the overall flow characteristics. The relative permeabilities $k_{rw}(S)$ and $k_{ro}(S)$ for the wetting and non-wetting phases vary with saturation S. The dynamic viscosities μ_w and μ_o correspond to the wetting and non-wetting phases. The pressures p_w and p_o refer to the wetting and non-wetting phases. This formulation does not account for gravity effects, which would require adding gravity to the pressure gradient.

The continuity equation represents the conservation of mass, where changes in saturation over time t are related to the divergence of the flow [14]. This relation is expressed as:

$$\phi\frac{\partial S_\alpha}{\partial t} + \frac{\partial v_\alpha}{\partial x} = 0 \tag{2}$$

where ϕ stands for the porosity of the medium, S_α the saturation of phase α, and v_α the volumetric flux of phase α.

In the case of incompressible flow, the total flux $v_T = v_w + v_n$ is constant, and the sum of the wetting and non-wetting phase saturations $S_w + S_n = 1$. Additionally, the pressure difference between the wetting and non-wetting phases $(p_n - p_w)$ is related to the capillary pressure:

$$P_c = p_n - p_w \tag{3}$$

In this paper, the relative permeability and capillary pressure are functions of saturation only, i.e., $k_{r,\alpha} \equiv k_{r,\alpha}(S_w)$ and $p_c \equiv p_c(S_w)$ [15, 16]. The time evolution of $S_w(x,t)$ can be computed by combining governing Eqs. (1)–(3). In that process, the fractional flow f_w is defined as:

$$f_w = \frac{\lambda_w}{\lambda_w + \lambda_n} = \frac{1}{1 + \frac{k_{r,n}/\mu_n}{k_{r,w}/\mu_w}} \tag{4}$$

Combination of Eq. (1)-(4) leads to which describes the evolution of $S_w(x,t)$ in space and time.

$$\phi\frac{\partial S_w}{\partial t} + \frac{\partial}{\partial x}\left[f_w v_T\right] + \frac{\partial}{\partial x}\left[f_w\lambda_n\frac{\partial p_c}{\partial x}\right] = 0 \tag{5}$$

In this work, Eq. (5) is solved numerically. From the numerical solution the production curve (Eq. 6)

$$Q(t) = \int_0^L S_w(x,t)\,dx \tag{6}$$

can be computed by integrating the saturation profile over the computational domain in x, utilizing the concept of mass conservation [15].

2.2 Relative permeability model

Lomeland et al. [9] proposed the concept of relative permeability being dependent on saturation functions, and more recent studies have further refined these models, incorporating additional parameters to enhance predictive capabilities [2, 9, 17]. Relative permeability is typically assumed to be a function of saturation $k_{r,\alpha}(S_w)$. The reduced saturation $\hat{S}_w$ is expressed as,

$$\hat{S}_w = \frac{S_w - S_{wi}}{1 - S_{or} - S_{wi}} \tag{7}$$

where saturation S_w is re-scaled to the range between irreducible wetting saturation S_{wi} and residual non-wetting phase saturation S_{or} [17].

For water-oil flow, the proposed correlation is described by three parameters: L_o^w, E_o^w, T_o^w, where the subscript o denotes the oil phase, and the superscript w denotes the water phase. The correlation for oil and water relative permeability with water injection is then given by:

$$k_{ro}(S_w) = k_{ro}^w \frac{(1-\hat{S}_w)^{L_o^w}}{(1-\hat{S}_w)^{L_o^w} + E_o^w \hat{S}_w^{T_o^w}}, \quad k_{rw}(S_w) = k_{rw}^o \frac{\hat{S}_w^{\,L_w^o}}{\hat{S}_w^{L_w^o} + E_w^o (1-\hat{S}_w)^{T_w^o}} \tag{8}$$

where only the parameters S_{wi}, S_{or}, k_{rw}^o, and k_{ro}^w have physical meaning, while the parameters L, E, and T are empirical and describe the lower part, slope, and upper part of the curve, respectively [9].

This model was developed to capture variations in behavior across the entire range of water saturation. Experimental results have demonstrated the model's accuracy in interpreting data over a wide range of saturations [2].

The LET model was used to parameterize the study, which included experimental data such as the NP and ΔP between the water inlet and the oil/water outlet. In addition, the capillary pressure —which was also parameterized using the LET model— was taken into account to optimize the core flooding data.

2.3 Datasets

The data analyzed in this study was obtained from a core-flooding experiment conducted under controlled laboratory conditions, including atmospheric pressure, room temperature, and the use of mineral oil. The experiment was performed in transient regime, where one fluid is displaced from the porous medium by injecting another fluid at a constant flow rate or constant pressure. The dataset from the Sample BB1 described in Table 1.

Table 1. Summary of physical and wettability properties for Sample BB1

Parameter/Property	Sample BB1	Unit	Parameter/Property	Sample BB1	Unit
Lithology	Buff Berea	-	Oil density	0.850	g/cm³
Porosity	0.227	-	Core length	4.84	cm
Absolute Permeability	602	mD	Core diameter	3.82	cm
Water viscosity	1.480	cp	Swi	18.71	%
Oil viscosity	4.800	cp	Wettability regime	Water-wet	-
Water density	1.142	g/cm³			

2.4 Local Sensitivity Analysis Method

Sensitivity analysis is an essential technique for understanding how variations in a model's parameters affect its state variables. This analysis utilizes the Jacobian matrix, which consists of the partial derivatives of the state variables with respect to the model parameters. The Jacobian matrix, **J**, is defined as,

$$J_{ij} = \frac{\partial W_i}{\partial \theta_j} \tag{9}$$

where W_i represents the i-th state variable and θ_j represents the j-th parameter. This approach allows quantifying the sensitivity of each state variable to changes in each parameter, providing valuable insights for model calibration and robustness [18].

To assess the sensitivity of the state variable concerning the analyzed parameter, the reduced sensitivity coefficient of relative sensitivity X_{θ_j} is calculated by differentiating the state variable with respect to the parameter and multiplying this derivative by the parameter value. Equation 9 can be approximated using a central difference scheme [19]. In this work, $\epsilon = 10^{-3}$.

$$X_{\theta_j} = \theta_j \frac{\partial \mathbf{W}}{\partial \theta_j} \approx \frac{W_i(\theta_1, \theta_2, \ldots, \theta_j + \epsilon\theta_j, \ldots, \theta_{N_{\text{par}}}) - W_i(\theta_1, \theta_2, \ldots, \theta_j - \epsilon\theta_j, \ldots, \theta_{N_{\text{par}}})}{2\epsilon} \tag{10}$$

The commercial software Cydar® [10]was used to optimized the relative permeability parameters using experimental data. These adjustments enabled a local sensitivity analysis of $S_w(x,t)$, ΔP, and NP curves. The objective was to assess the impact of each parameter on the final results, highlighting the relative significance of each component in result variability. The resulting data were then analyzed about the computed sensitivity indices, with particular attention to any potential correlations or differences between various sensitivity analysis techniques.

3 Results and Discussion

3.1 Relative Permeability Optimization via Cydar

The following visual representations in Fig. 1 were generated in Cydar® as a result of applying this method:

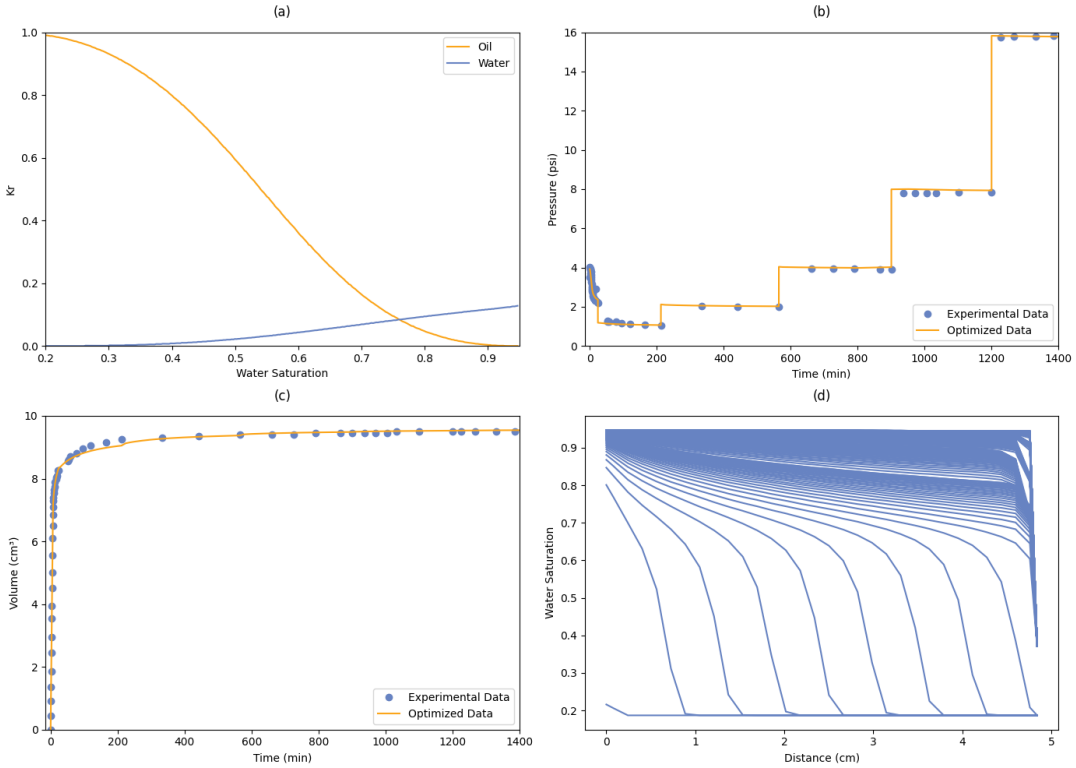

Figure 1. Optimization results using Cydar®: (a) Relative Permeability Curve, (b) Pressure differential between water inlet and oil and water outlet (ΔP) (c) Cumulative production (NP), and (d) Water Saturation Curve.

Figure 1a shows the relationship between water saturation and the relative permeability of oil and water. As

water saturation increases, the relative permeability of oil decreases, reflecting the progressive replacement of oil by water in the reservoir pores [20]. Figure 1b details the pressure difference (ΔP) over time, where the "bumps" represent stages of pressurization and stabilization. Each abrupt increase in pressure suggests the application of a new injection phase or operational adjustment, aiming to maintain the efficiency of fluid displacement [21]. Figure 1c illustrates the cumulative production (NP), indicating a rapid initial increase followed by stabilization, common in production processes where initial pressure drives high production that eventually balances out [22]. Finally, Figure 1d shows the water saturation profile along the distance, indicating how the water advances through the reservoir.

3.2 Reduced Sensitivity Coefficient Analysis

In this section, Figs. 2, 3, and 4 present the reduced sensitivity coefficients. On Figure 2 illustrates the reduced sensitivity coefficients of $S_w(x,t)$ at various dimensionless positions within the sample (X = 0.1, 0.5, 0.9). On the other hand, Fig. 3 and 4 shows, respectively, the reduced sensitivity coefficients of NP and ΔP.

3.2.1 Reduced Sensitivity Coefficient of Water Saturation

On Fig. 2, an analysis of the reduced sensitivity coefficients of $S_w(x,t)$ with regard to parameters Lw and Lo is presented (Fig. 2a), Ew and Eo (Fig. 2b), and Tw and To (Fig. 2c). Considering the reduced sensitivity coefficient of saturation at three dimensionless positions (X = 0.1, 0.5, 0.9), it can be observed that in Figure 2a, the parameter Lw shows no significant sensitivity throughout the experiment duration. In contrast, Lo stands out due to its maximum sensitivity variation at 25 minutes from the start of the experiment and maintains non-zero sensitivity until the end, indicating its continuous importance throughout the process, albeit with reduced magnitude. In Figure 2b, parameters Ew and Eo show maximum sensitivity variation at 25 minutes, both becoming insensitive by 600 minutes, indicating that after a certain time, variations in these parameters have reduced or no impact on $S_w(x,t)$. In Figure 2c, similar to the behavior of Lo, Eo, and Ew, parameter To also shows maximum sensitivity variation at the start of the experiment, becoming insensitive by 400 minutes, and the reduced sensitivity coefficient for Tw shows irrelevant sensitivity throughout the experiment. It is worth noting that the positions at the end of the samples exhibit higher sensitivity. Specifically, the X = 0.9 position, where water saturation is most sensitive to the parameters under analysis, is followed by positions X = 0.5 and X = 0.1.

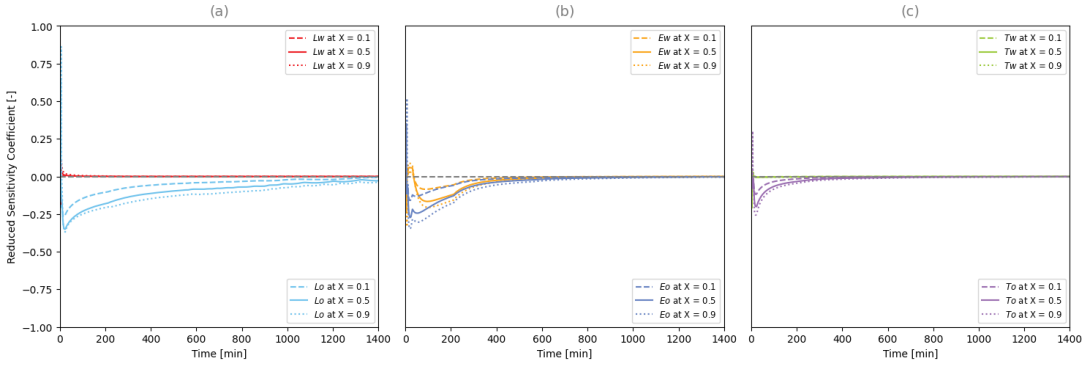

Figure 2. Reduced Sensitivity Coefficiente of Water Saturation

3.2.2 Reduced Sensitivity Coefficient of NP

On Figure 3, depicts an analysis of the reduced sensitivity coefficients of NP regarding the parameters Lw and Lo (Fig. 3a), Ew and Eo (Fig. 3b), and Tw and To (Fig. 3c). Given the reduced sensitivity coefficient of NP, in Figure 3a, parameters Lw and Lo stand out with maximum sensitivity variation at 10 and 25 minutes from the start of the experiment, respectively. It is also noted that Lw becomes insensitive by 200 minutes, while Lo maintains non-zero sensitivity until the end, indicating its continuous importance throughout the process, albeit with reduced magnitude. In Figure 3b, parameters Ew and Eo similarly show maximum sensitivity variation at 25 minutes from the start of the experiment, becoming insensitive by 1000 and 1200 minutes, respectively. In Figure 3c, it is observed that parameter Tw exhibits a new maximum variation in sensitivity as the "bumps" occur (Fig. 1c), while parameter To shows maximum variation at 10 minutes and becomes insensitive by 200 minutes.

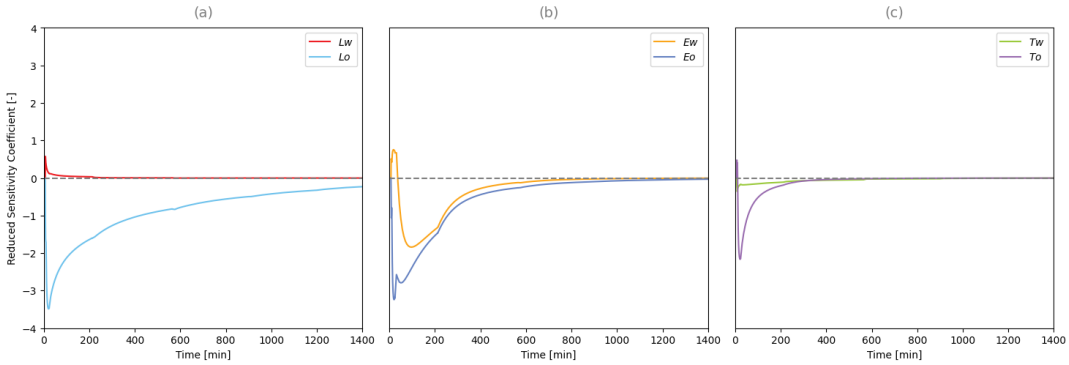

Figure 3. Reduced Sensitivity Coefficiente of NP

3.2.3 Reduced Sensitivity Coefficient of ΔP

On Fig. 4, an analysis of the reduced sensitivity coefficients of ΔP is presented with respect to the parameters Lw and Lo (Fig. 4a), Ew and Eo (Fig. 4b), and Tw and To (Fig. 4c). In Fig. 4a, parameter Lo shows a new variation in sensitivity as "bumps" occur (Fig. 1c), with maximum variations at 800 minutes and again at 1000 minutes, while parameter Lw exhibits maximum variation in the early minutes of the experiment and becomes insensitive at 50 minutes. Fig. 4b demonstrates that parameters Ew and Eo similarly show the influence of "bumps" (Fig. 1c) on a reduced scale, remaining sensitive throughout the experiment. In Fig. 4c, it was found that Tw and To have maximum variation at 25 minutes and become insensitive by 600 minutes.

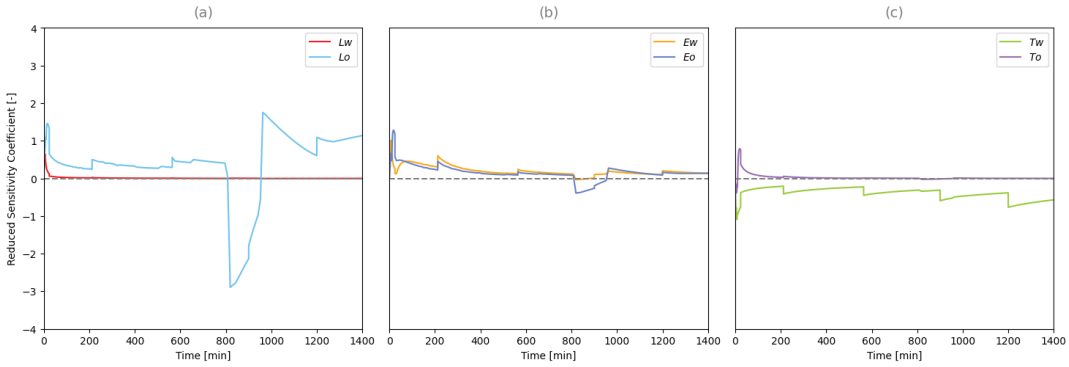

Figure 4. Reduced Sensitivity Coefficiente of ΔP

4 Conclusions

This study investigated the sensitivity analysis of relative permeability parameters using the LET model in unsteady-state water injection experiments. The methodology combined experimental data with computational simulations to optimize relative permeability and capillary pressure. Optimization using Cydar® [10] showed excellent agreement between experimental data and simulations. The reduced sensitivity coefficient of $S_w(x,t)$ at the three dimensionless positions considered (X = 0.1, 0.5, 0.9), four sensitive parameters were identified: Lo, To, Eo, and Ew, which stood out due to the maximum variation in sensitivity at 25 minutes from the start of the experiment. The remaining two parameters, Lw and Tw, did not show relevant sensitivity throughout the duration of the experiment. It was observed that To, Eo, and Ew become insensitive at 400, 600, and 600 minutes, respectively, and that Lo exhibits non-zero sensitivity until the end of the experiment, albeit with reduced magnitude.

Considering the reduced sensitivity coefficient of NP, the parameters: Lo, To, Eo, Lw, and Ew, have a similar behavior to the reduced sensitivity parameters of saturation, which stand out due to the maximum variation in sensitivity at 25 minutes into the experiment, except for the parameter Lw, which has its maximum variation at 10 minutes from the start of the experiment. The sixth sensitive parameter, Tw, was observed to have a new maximum variation in sensitivity as the "bumps" occur. It was observed that Lw, Ew, Eo, and To become insensitive at 200, 1000, 1200, and 200 minutes, respectively, and that Lo exhibits non-zero sensitivity until the end of the experiment.

Throughout the experiment, it is observed that the reduced sensitivity of ΔP, indicates that the parameters Lo, To, Eo, and Ew are more sensitive compared to the parameters Lw and Tw. For the parameter Lo, it is noted that as "bumps" occur, there is a new variation in sensitivity, with maximum variations at 800 minutes and again at 1000 minutes. The parameter Lw becomes insensitive at 50 minutes. On a reduced scale, the same behavior is observed for the parameters Ew and Eo, which also show the influence of "bumps", remaining sensitive all through the experiment, although with non-zero sensitivity but of reduced magnitude. It was found that Tw and To have maximum variation at 25 minutes and become insensitive at 600 minutes, indicating that after a certain time, variations in these parameters have reduced or no impact on ΔP.

Thus, the proposed method for conducting reduced sensitivity coefficient analyses provided a detailed understanding of the behavior of LET parameters during core flooding experiments. The identification of the most sensitive parameters allowed focusing on those with the greatest impact, optimizing the accuracy and efficiency of the model. This method not only improves the reliability of experimental results but also has the potential to reduce the time and resources needed for future experiments.

Acknowledgements. This research was carried out in association with the ongoing R&D project registered as ANP nº 24.551, "Avaliação de Metodologias para Interpretação de Curvas de Permeabilidade Relativa em meios porosos heterogêneos " (UFRJ/Petrobras Brasil/ANP), sponsored by Petróleo Brasileiro S/A under the ANP R&D levy as "Compromisso de Investimentos com Pesquisa e Desenvolvimento".

This research was financially supported by the Human Resources Program of the National Agency of Petroleum, Natural Gas, and Biofuels – PRH-ANP, supported with resources from the investment of qualified oil companies under the R&D Clause of ANP Resolution No. 50/2015.

This study was financed, in part, by the São Paulo Research Foundation (FAPESP), Brasil. Process Number 2024/11265-0.

References

[1] E. D. NASCIMENTO. *Estudo paramétrico para modelagem e simulação computacional de reservatórios carbonáticos em sub-sal*. PhD thesis, Dissertação M. Sc., COPPE/UFRJ, Rio de Janeiro, RJ, Brasil, 2010.

[2] D. CAPRA. Relative permeability models: a systematic sensitivity analysis, 2020.

[3] A. Saltelli. Sensitivity analysis for importance assessment. *Risk analysis*, vol. 22, n. 3, pp. 579–590, 2002.

[4] J. Morio. Global and local sensitivity analysis methods for a physical system. *European journal of physics*, vol. 32, n. 6, pp. 1577, 2011.

[5] E. Borgonovo. *Sensitivity analysis: an introduction for the management scientist*, volume 251. Springer, 2017.

[6] F. Pianosi, K. Beven, J. Freer, J. W. Hall, J. Rougier, D. B. Stephenson, and T. Wagener. Sensitivity analysis of environmental models: A systematic review with practical workflow. *Environmental Modelling & Software*, vol. 79, pp. 214–232, 2016.

[7] G. d. M. Stieven, D. d. R. Soares, E. P. Oliveira, and E. F. Lins. Interfacial heat transfer coefficient in unidirectional permanent mold casting: Modeling and inverse estimation. *International Journal of Heat and Mass Transfer*, vol. 166, pp. 120765, 2021.

[8] S. Tarantola, F. Ferretti, S. L. Piano, M. Kozlova, A. Lachi, R. Rosati, A. Puy, P. Roy, G. Vannucci, M. Kuc-Czarnecka, and others. An annotated timeline of sensitivity analysis. *Environmental Modelling & Software*, vol. 174, pp. 105977, 2024.

[9] F. Lomeland, E. Ebeltoft, and W. H. Thomas. A new versatile relative permeability correlation. In *International symposium of the society of core analysts, Toronto, Canada*, volume 112, 2005.

[10] Cydarex. *CYDAR User Guide*. Cydarex, 2024.

[11] J. Bear. *Dynamics of fluids in porous media*. Courier Corporation, 2013.

[12] Z. Chen, G. Huan, and Y. Ma. *Computational methods for multiphase flows in porous media*. SIAM, 2006.

[13] M. Leverett. Capillary behavior in porous solids. *Transactions of the AIME*, vol. 142, n. 01, pp. 152–169, 1941.

[14] G. K. Batchelor. *An introduction to fluid dynamics*. Cambridge university press, 2000.

[15] S. Berg, H. Dijk, E. Unsal, R. Hofmann, B. Zhao, and V. R. Ahuja. Simultaneous determination of relative permeability and capillary pressure from an unsteady-state core flooding experiment? *Computers and Geotechnics*, vol. 168, pp. 106091, 2024.

[16] A. Yekta, J.-C. Manceau, S. Gaboreau, M. Pichavant, and P. Audigane. Determination of hydrogen–water relative permeability and capillary pressure in sandstone: application to underground hydrogen injection in sedimentary formations. *Transport in Porous Media*, vol. 122, n. 2, pp. 333–356, 2018.

[17] S. Berg, E. Unsal, and H. Dijk. Sensitivity and uncertainty analysis for parameterization of multiphase flow models. *Transport in Porous Media*, pp. 1–31, 2021.
[18] A. Saltelli. Global sensitivity analysis: an introduction. In *Proc. 4th International Conference on Sensitivity Analysis of Model Output (SAMO'04)*, volume 27, pp. 43. Citeseer, 2004.
[19] H. R. Orlande. *Inverse heat transfer: fundamentals and applications*. CRC Press, 2021.
[20] T. Ahmed. *Reservoir engineering handbook*. Gulf professional publishing, 2018.
[21] T. Ahmed and P. McKinney. *Advanced reservoir engineering*. Elsevier, 2011.
[22] L. P. Dake. *Fundamentals of reservoir engineering*. Elsevier, 1983.